

# Experimental Modal Analysis on Full-Field DSLR Camera Footage Using Spectral Optical Flow Imaging

Jaka Javh<sup>a</sup>, Janko Slavič<sup>a,\*</sup>, Miha Boltežar<sup>a</sup>

<sup>a</sup>*University of Ljubljana, Faculty of Mechanical Engineering, Aškerčeva 6, 1000 Ljubljana, Slovenia*

*Cite as:*

*Jaka Javh, Janko Slavič, Miha Boltežar, Experimental modal analysis on full-field DSLR camera footage using spectral optical flow imaging, Journal of Sound and Vibration, Volume 434, 2018, Pages 213-220, ISSN 0022-460X, <https://doi.org/10.1016/j.jsv.2018.07.046>.*

---

## Abstract

High-speed camera measurements are increasingly being used in modal analysis to instantaneously measure full-field structural responses by extracting the displacement information from images using digital-image-correlation and other optical-flow methods. High-speed cameras capable of filming full frame at high frame rates can be very expensive and produce image resolutions of only approximately 1 mega pixel, which is why this research aims at measuring and identifying the full-field response using cheaper, still-frame cameras with a higher image and intensity resolution, such as digital single-lens reflex (DSLR) and mirrorless cameras. Using spectral optical flow imaging (SOFI) full-field operational shapes can be acquired using still-frame cameras. This study demonstrates the hybrid modal-parameter identification of full-field mode shapes using an accelerometer and a DSLR camera for responses far above the DSLR camera's frame rate (demonstrated up to 1 kHz).

*Keywords:* SOFI, DSLR camera, modal-parameter identification, optical flow, LSFD, Photogrammetry

---

---

\*Corresponding author

*Email address:* [janko.slavic@fs.uni-lj.si](mailto:janko.slavic@fs.uni-lj.si) (Janko Slavič)

## 1. Introduction

Displacements can be tracked in videos by monitoring the pixel-intensity variations [1] using optical flow algorithms such as the Lucas-Kanade method [2] (commonly referred to as digital image correlation) with displacement resolutions typically quoted at around 1/100 of a pixel frame-to-frame and 1/10000 of a pixel in the amplitude spectrum for longer time series [1]. High-speed cameras are increasingly being used in modal analyses because of their many advantages [3]: the measurements are non-contact and do not affect the measured structure with any dummy mass. In addition, by using cameras the entire full-field is measured instantaneously and not by scanning the surface over time, like in the case with scanning-laser vibrometers [4], enabling measurement of rotating structures as well [5]. Lastly, because cameras measure displacements, lower-frequency oscillations with larger motions (in the range of centimetres to metres), as is often the case with large structures [6], can be measured, opening possibilities for structural health monitoring [7].

A limitation when using measurements based on high-speed cameras is the price, which can range up to a couple of hundred thousand euro for high-end stereoscopic (3D) measurement set-ups. Lower-frame-rate cameras are much less expensive, which is why many research papers describe attempts to measure dynamic responses with such cameras. One such example is the use of a mobile-phone camera to measure a stay cable's natural frequency and in turn its tension [8]. Under-sampling and re-mapping the time instances can be implemented to measure above the Nyquist frequency [9], as well as by setting a short exposure time and using frequency zooming, thereby allowing for aliasing [10]. Another possibility is filming at different frame rates and combining the information to produce the aliased spectrum [11]. Furthermore, the rolling-shutter effect has been used to sample high frequencies from a normal DSLR camera video [12]. As explained in [10] aliasing approaches from [9–11] and the use of the rolling-shutter [12] require very short exposure times, since longer exposures act as temporal filters producing a sort of low-pass filtering. Aliasing approaches are somewhat limited by this short exposure requirement in that little light can be captured without the use of strobe lights, which produce an intense but short pulse of light, resulting in an image with little-to-no blur [13]. The paper [14] is an example of using strobe lights to measure the dynamics of an oscillating wing in 3D using multiple viewpoints and [15] uses strobe lights to measure at higher frequencies. Due to the time invariance of linear system responses, stereoscopic

information can be acquired with repeated measurements at different angles [16, 17] or by using a dividing mirror, producing two viewing angles [18], thereby requiring only one camera instead of two. Lower-frame-rate cameras typically achieve lower image-noise values, a higher image resolution and higher dynamic range. For instance, DSLR and mirrorless cameras in the 500–2000 euro price range typically boast a 14-bit colour-intensity resolution and a 24 mega-pixel count.

It was recently shown that images indicating individual displacement spectral components can be produced by harmonically varying the illumination, thereby producing an analogue Fourier transform [19]. This method, known as spectral optical flow imaging (SOFI), can obtain operational displacement shapes using still-frame cameras such as DSLR or mirrorless cameras, by acquiring a reference image, an image with a sine phase and an image with a cosine phase, and then combining the information into a full-field complex displacement field for a chosen frequency, determined by the harmonic of the blinking lights.

In another publication [20] a hybrid modal-parameter identification was used to combine eigenvalues measured by an accelerometer and full-field mode shapes measured by a high-speed camera, making it possible to identify mode shapes below the camera’s noise floor up to 10 kHz.

This research implements SOFI measurements to acquire high-frequency full-field displacement fields for selected frequencies up to 1 kHz and combines this data in the hybrid modal-parameter identification from [20], where by using the least-squares complex-frequency method (LSCF) [21] to identify the eigenvalues from a single point sensor (accelerometer and/or laser vibrometer) and using the least-squares frequency-domain method (LSFD) [22] on the SOFI measurements, the full-field mode shapes are produced.

## 2. Spectral Optical Flow Imaging

Spectral optical flow imaging (SOFI) was introduced in [19]. In this section the method is briefly explained. For more on the method, please refer to the original publication.

An object reflects light  $L$  from a surface pattern with a reflectance  $P(x, y)$  (where  $(x, y)$  are the coordinates of the camera’s image plane) producing a radiance field  $r((x, y), L)$ :

$$r((x, y), L) = P(x, y) L \tag{1}$$

A camera produces an image with intensity values  $I(x, y)$  by integrating the radiance falling on individual pixels over the camera's exposure time  $T_e$ :

$$I((x, y), L) = \int_0^{T_e} r((x, y), L) dt, \quad (2)$$

By assuming small displacements, a displacement  $s$  will produce a change in the radiance approximately equal to:

$$r((x, y) + s, L_0) = r((x, y), L_0) + s \nabla r((x, y), L_0), \quad (3)$$

where  $\nabla r$  is the radiance gradient. The produced relation is based on brightness conservation and is used to estimate the displacements in gradient-based optical flow such as Lucas-Kanade [1, 2]. The equation is typically written in the form of pixel intensities instead of radiance.

By additionally incorporating a harmonically varying illumination  $L(t) = L_0 + L_A \sin(\omega_l t)$  the radiance can be expressed as:

$$\begin{aligned} r((x, y) + s((x, y), t), L(t)) &= \frac{L(t)}{L_0} r((x, y) + s((x, y), t), L_0) = \\ &= \frac{L(t)}{L_0} \left( r((x, y), L_0) + s((x, y), t) \nabla r((x, y), L_0) \right) \end{aligned} \quad (4)$$

By integrating both sides of the equation (4) over the exposure time  $T_e$  and neglecting non-significant terms, the following relation can be produced:

$$\begin{aligned} \underbrace{I((x, y) + s((x, y), t), L(t))}_{\text{blinking \& vibrations image}} &= \underbrace{I((x, y), L_0)}_{\text{reference image}} + \\ + \underbrace{\frac{L_A}{L_0}}_{\text{illumination scaling}} &\underbrace{\nabla I((x, y), L_0)}_{\text{reference image gradient}} \underbrace{\frac{S_s((x, y), \omega_l)}{2}}_{\text{displacement spectral component}} \end{aligned} \quad (5)$$

the above equation indicates that an image of a vibrating structure illuminated with a harmonically varying light (blinking & vibrations image) is composed of a motionless image under constant illumination (reference image) and the distortion caused by the displacement spectral component, which is a product of the illumination scaling, the reference image gradient and the

displacement spectral component  $S_s((x, y), \omega_l)$  of the frequency equal to the frequency of the varying light  $\omega_l$ .

By subtracting the reference image from the blinking & vibrations image and scaling the result with the reference image gradient and the illumination scaling, a displacement spectral component  $S_s((x, y), \omega_l)$  can be obtained for every pixel:

$$S_s((x, y), \omega_l) = \frac{I\left((x, y) + s((x, y), t), L(t)\right) - I((x, y), L_0)}{\frac{1}{2} \frac{L_A}{L_0} \nabla I((x, y), L_0)} \quad (6)$$

By using different frequencies for the blinking lights, other spectral components can be measured, also by changing the phase of the lights from  $\sin(\omega_l t)$  to  $\cos(\omega_l t)$  the cosine amplitudes  $S_c((x, y), \omega_l)$  can be measured. The frequency of interest is not limited by the camera and can be very high (in the range of kHz) as long as the displacements are significant enough (above the noise floor) to be identified. Relatively small displacement amplitudes can be measured, because a typical displacement resolution between two images is in the range of a hundredth of a pixel, provided that the gradient in the pixel  $(x, y)$  is appropriate [1].

The principle of measuring individual spectral components using SOFI is analogous to the Fourier transform and is equally affected by windowing effects and spectral leakage [23]. To avoid windowing effects, the exposure time  $T_e$  should preferably match multiples of the displacement and illumination harmonic periods.

The displacement amplitudes  $S_s((x, y), \omega_n)$  and  $S_c((x, y), \omega_n)$  are displacements in the direction of the image gradient only. The 2D displacements can be obtained using Lucas-Kanade by solving the system of equations for a  $H \times H$  subset containing various gradient directions:

$$\begin{Bmatrix} \Delta x \\ \Delta y \end{Bmatrix} = \begin{bmatrix} \sum (\frac{\partial I_0}{\partial x})^2 & \sum (\frac{\partial I_0}{\partial x} \frac{\partial I_0}{\partial y}) \\ \sum (\frac{\partial I_0}{\partial x} \frac{\partial I_0}{\partial y}) & \sum (\frac{\partial I_0}{\partial y})^2 \end{bmatrix}^{-1} \begin{Bmatrix} \sum ((I_1 - I_0) \frac{\partial I_0}{\partial x}) \\ \sum ((I_1 - I_0) \frac{\partial I_0}{\partial y}) \end{Bmatrix}, \quad (7)$$

where  $I_0$  is the reference image,  $I_1$  is the translated image,  $\partial I/\partial x$  indicates the gradient in the  $x$  direction and likewise  $y$ ,  $\Delta x$  and  $\Delta y$  are the  $x$  and  $y$  displacement components and the summations indicate the convolutions over the subset:

$$\sum \left( \frac{\partial I_0}{\partial x} \frac{\partial I_0}{\partial y} \right) = \sum_{k=-\frac{H}{2}}^{\frac{H}{2}} \sum_{l=-\frac{H}{2}}^{\frac{H}{2}} \left( \frac{\partial I_0}{\partial x}(x+k, y+l) \frac{\partial I_0}{\partial y}(x+k, y+l) \right) \quad (8)$$

In the case of SOFI, to obtain the 2D displacement components  $X_s((x, y), \omega_l)$  and  $Y_s((x, y), \omega_l)$ , image  $I\left((x, y) + s((x, y), t), L(t)\right)$  should be used in place of  $I_1$  and the reference image  $I\left((x, y), L_0\right)$  should be used in place of  $I_0$ . Also, the result has to be scaled according to the illumination  $1/(L_A/L_0)$ .

### 3. Hybrid Modal-parameter identification

A structure's dynamic response  $x_j(t)$  at position  $j$  for excitation in position  $k$  is a linear combination of the modal coordinates [24]:

$$x_j(t) = \sum_r {}_r A_{jk} e^{\lambda_r t}, \quad (9)$$

where  ${}_r A_{jk}$  is the modal constant value for location  $j$  and represents the spatial scaling. Modal constants represent the scaled mode shapes, as mode shapes are otherwise non-dimensional.  $e^{\lambda_r t}$  is the complex exponential time response with an eigenvalue  $\lambda_r = -\zeta_r \omega_r \pm i \omega_r \sqrt{1 - \zeta_r^2}$  for the  $r$ -th mode, where  $\omega_r$  and  $\zeta_r$  are the eigenfrequency and the modal damping coefficient. As is clear from the  $\pm$  in front of the imaginary part,  $\lambda_r$  comes in conjugate pairs, one with a modal constant  ${}_r A_{jk}$  and the other with its conjugate pair  ${}_r A_{jk}^*$ .

Modal-parameter identification methods typically identify the eigenvalues and the mode shapes separately. By using the least-squares complex-frequency (LSCF) [21] identification method, stabilization diagrams can be produced and the eigenvalues picked from them. The identification is then continued with the least-squares frequency-domain (LSFD) [22] identification method to identify the mode shapes.

Since the time response is global (9), only one location has to be measured to obtain the eigenvalues  $\lambda_r$  (that is if the value  ${}_r A_{jk}$  for the chosen measured location  $j$  and excitation  $k$  is  $\neq 0$  for all  $r$ ). By using a precise sensor, such as an accelerometer or a laser vibrometer, eigenvalues can be identified from a single point measurement ( $\hat{\lambda}_r$  for  $r = 1, 2, \dots, N$ ).

After knowing the eigenvalues, selected full-field frequency components of interest can be measured using SOFI and the full-field mode shapes identified with the LSFD method. LSFD identifies the modal constants  ${}_r A_{jk}$  based on the response model [25]:

$$\alpha_{jk}(\omega) = \sum_{r=1}^N \left( \frac{{}_r A_{jk}}{i \omega - \lambda_r} + \frac{{}_r A_{jk}^*}{i \omega - \lambda_r^*} \right) - \frac{R_L}{\omega^2} + R_U \quad (10)$$

$R_L$  and  $R_U$  are the optional lower and upper residuals.

Using measured full-field (SOFI) frequency responses  $\hat{\alpha}_{jk}(\Omega_n)$ , where  $\Omega_n$  are the selected measured angular frequencies of interest, a system of linear equations can be produced using the equation (10):

$$\begin{pmatrix} \hat{\alpha}_{jk}(\Omega_1) \\ \hat{\alpha}_{jk}(-\Omega_1) \\ \hat{\alpha}_{jk}(\Omega_2) \\ \vdots \\ \hat{\alpha}_{jk}(-\Omega_L)^* \end{pmatrix} = \begin{bmatrix} \frac{1}{i\Omega_1 - \hat{\lambda}_1} & \frac{1}{-i\Omega_1 - \hat{\lambda}_1^*} & \frac{1}{i\Omega_1 - \hat{\lambda}_2} & \cdots & \frac{1}{-i\Omega_1 - \hat{\lambda}_N^*} \\ \frac{1}{i\Omega_2 - \hat{\lambda}_1} & \frac{1}{-i\Omega_2 - \hat{\lambda}_1^*} & \frac{1}{i\Omega_2 - \hat{\lambda}_2} & \cdots & \frac{1}{-i\Omega_2 - \hat{\lambda}_N^*} \\ \vdots & \vdots & \ddots & \vdots & \vdots \\ \frac{1}{i\Omega_L - \hat{\lambda}_1} & \frac{1}{-i\Omega_L - \hat{\lambda}_1^*} & \frac{1}{i\Omega_L - \hat{\lambda}_2} & \cdots & \frac{1}{-i\Omega_L - \hat{\lambda}_N^*} \end{bmatrix} \begin{pmatrix} 1A_{jk} \\ 1A_{jk}^* \\ 2A_{jk} \\ \vdots \\ NA_{jk}^* \end{pmatrix} \quad (11)$$

The solution of the above system produces the modal constants (mode shapes) and residuals. For  $N$  conjugate eigenvalue pairs ( $2N$ ) at least  $N$  complex response frequency points have to be measured to produce  $N$  conjugate modal constant pairs ( $2N$ ).  $N$  frequency points are conjugated to produce an additional  $N$  negative frequency points  $\hat{\alpha}_{jk}(-\Omega_1) = \hat{\alpha}_{jk}(\Omega_1)^*$ , combining to produce  $2N$  equations forming the system in Eq. (11). An inverse can be determined once and used to calculate the modal constants for each excitation and response location  $jk$ .

#### 4. Experiment and practical considerations

An experiment using a cymbal as the test structure was performed. A cymbal was chosen because it has a wideband dynamic response and has been measured extensively in previous experiments [1, 19].

Since SOFI only works for small displacements and is sensitive to large rigid-body motions, the cymbal was rigidly fixed at its centre hole and a stinger for shaker excitation was attached close to the ridge of the cymbal's inner indentation (see Figure 1).

A simple light regulating the circuit was used to harmonically regulate the light intensity and the experiment was performed in a dark (anechoic) chamber to avoid outside interference, such as ambient light.

The excitation was measured with a force transducer attached between the shaker and the cymbal. The response was measured with an accelerometer. Later, an additional response point was measured with a laser vibrometer, because the accelerometer placement failed to identify some mode shapes. The light intensity was measured as well, for the purposes of monitoring.

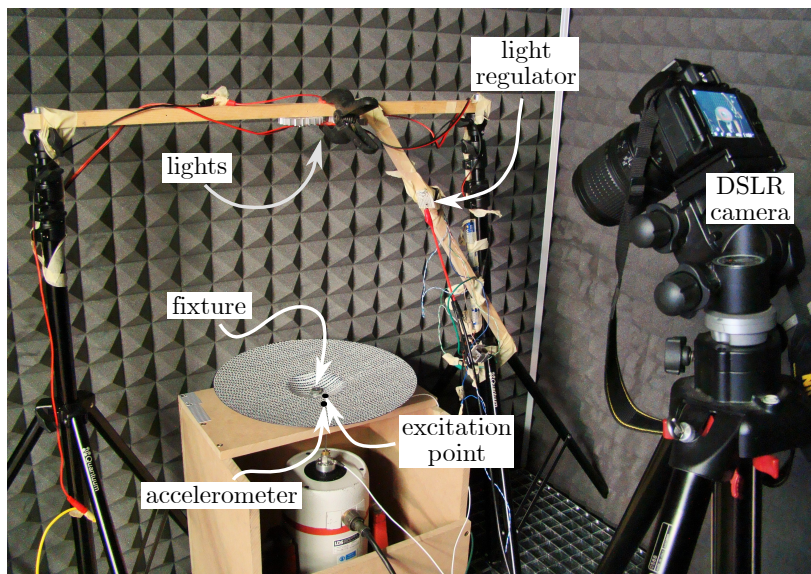


Figure 1: The SOFI experimental set-up using a consumer DSLR camera to measure a cymbals dynamic response to excitation with a shaker. The LED illumination and a regulating circuit are situated above the cymbal to produce the desired illumination.

The eigenvalue identification was performed on the accelerometer and laser vibrometer measurements for a regulated pseudo-random (multi-sine) excitation of a 2 s window with a 30-1000 Hz frequency band.

The full-field spectral response measurements were later performed using SOFI on a Nikon D5300 DSLR camera during single harmonic excitation for frequencies selected to be close to the peak responses from the accelerometer and laser vibrometer measurements (see Table 1 for a list of measured frequencies). These are used in the LSFID identification of the mode shapes. The responses measured close to the resonant frequencies are already good approximations of the mode shapes, however they still contain residuals of mode shapes close by, while the modes identified with LSFID do not.

Table 1: The selected frequencies in Hz for the SOFI measurement.

32.7	56.1	91.3	111.8	257.0	264.6	272.5	299.6	340.7	349.1
455.9	464.6	531.5	534.3	551.6	562.5	576.7	568.5	601.7	632.6
643.0	647.6	664.1	731.2	734.3	742.4	749.6	799.0	815.3	832.6
835.0	842.1	861.7	884.9	943.0	946.0	944.8	982.5	991.3	

A problem arose associated with ensuring the repeatability between separate images. Motion and image brightness variations were observed between images taken under identical conditions. The source of the brightness inconsistencies remains unclear; however, it could be avoided by normalising the brightness over the entire image. A greater problem was the apparent motion between sequential and supposed stationary images. After extensive testing on a vibro-isolated block the source of motion appeared to be the jerk caused by the retraction of the mirror and the operation of the mechanical shutter of the DSLR camera. The jerk causes slight displacements of the camera and more critically the lenses, causing slight shifts that result in zoom and other apparent displacement fields. Figure 2 shows an example of such apparent displacements. The displacements are typically in the range of 0.1 pixel, which is significant, since the intention is to measure in the range of 0.01 pixel or less. The problem was solved by filming a video instead of

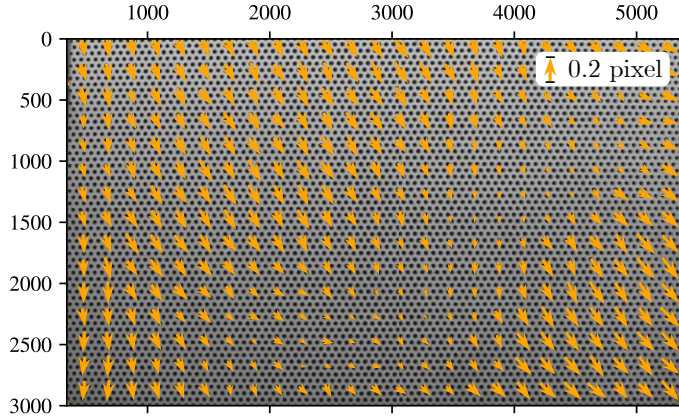


Figure 2: Example of the apparent displacement fields caused by the jerk of the camera shutter and/or the mirror retraction (a crop from a  $6000 \times 4000$  pixel image).

taking still images. A manual video setting of 50 fps and an exposure of  $1/50$  s was used to film the cymbal. By summing the  $1/50$  s frames of the 50 fps video an apparent still image could be produced, because no significant discontinuation of the intensity integration (2) is present between the video frames. An exposure  $T_e$  of approximately 0.5 s was required for a single still image to be used as SOFI. The exact exposure was tailored between 0.489 and 0.505 s to reduce the windowing effects. The exposure was controlled by setting the length of the illumination and turning the light off between separate images. To obtain the separate images the  $\approx 25$  frames of the video

during the illumination were summed and converted to black and white. Figure 3 shows one such still image produced from the video. Catching frames

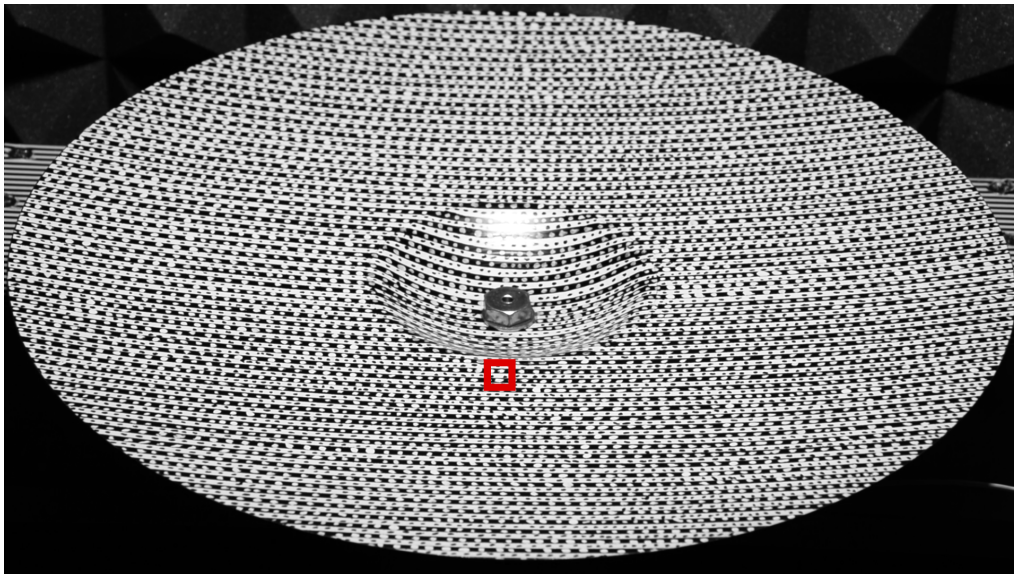


Figure 3: Image produced from the DSLR camera video (resolution  $1920 \times 1080$ ). The red square indicates the position of the accelerometer on the lower side of the cymbal.

from video is not the best solution, because the video is lossy compressed and the image resolution and bit depth are reduced, but the results proved to be very good, despite this.

The images for a selected frequency were taken in the following order. The single harmonic excitation was turned on and the cymbal started vibrating in the dark. Then a constant intensity light was shown for the set exposure time  $T_e$ , thereby producing the reference image. This was followed by a break in the illumination, then sine-phased harmonic light illumination for another period of  $T_e$ , and then cosine-phased harmonic illumination following that. The sequence of the three images (reference, sine, cosine) was repeated five times and later averaged to reduce the image noise. The film sequence was repeated for each chosen frequency. In order to be able to excite higher frequency responses with a greater intensity, the excitation used was single harmonic, otherwise SOFI can work with broad-band vibrations. Figure 4 shows the illumination and the excitation force during a SOFI measurement at 32.71 Hz. The illumination indicates the different segments of the measurement, i.e., the reference, sine and cosine images, repeated five

times.

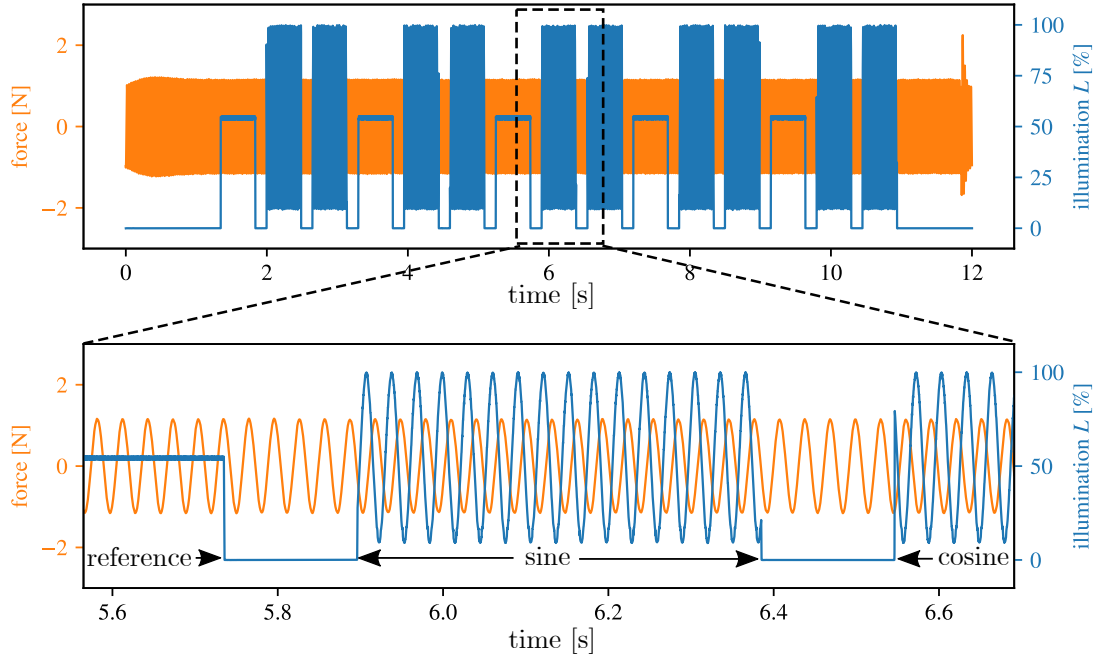


Figure 4: Measured illumination (blue) and force (orange) during five repetitions of a SOFI measurement at  $\Omega_0 = 2 \cdot \pi \cdot 32.71$ . The close-up illustrates the different illumination regimes.

The phase matching between the SOFI measurement and the force measurement is achieved by syncing the illumination with the excitation. Syncing was achieved by normalizing the full-field SOFI responses with the force amplitude, whose phase was determined with respect to the illumination phase. The normalization produces the full-field receptance values  $\alpha_{jk}(\Omega_n)$  for the chosen frequency  $\Omega_n$ .

## 5. Results

Figures 5 and 6 show some of the 39 mode shapes (modal constants) obtained from the SOFI measurement in the hybrid modal-parameter identification with the accelerometer eigenvalues. Each shape is accompanied by the identified eigenvalue in the form of an eigenfrequency  $f_r$  and damping  $\zeta_r$ . The plots are composed of arrows indicating the direction of the motion. The

density of the measured points can be very high (1739 point were measured in this example) and the arrows cannot be resolved in Figure 6, which is why Figure 5 is enlarged and composed of a reduced number of arrows. Green arrows are used to indicate the real values of the modal constants and the red arrows the imaginary values (colours available online). The intensity of the colours along with the size of the arrows indicate the magnitudes of the modal constant components.

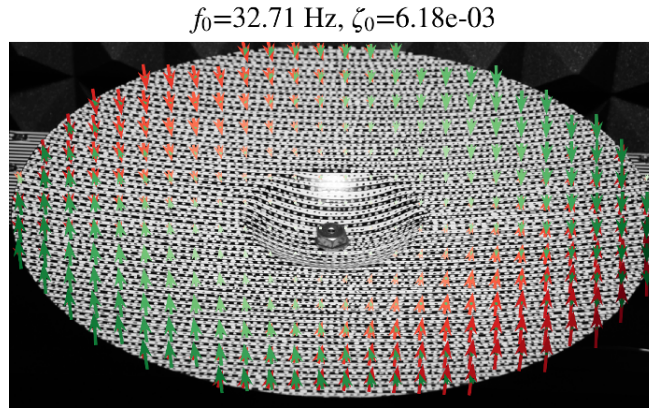


Figure 5: Large figure of an identified mode shape using SOFI. Green arrows indicate the direction and size of the real value components and red indicate the imaginary components.

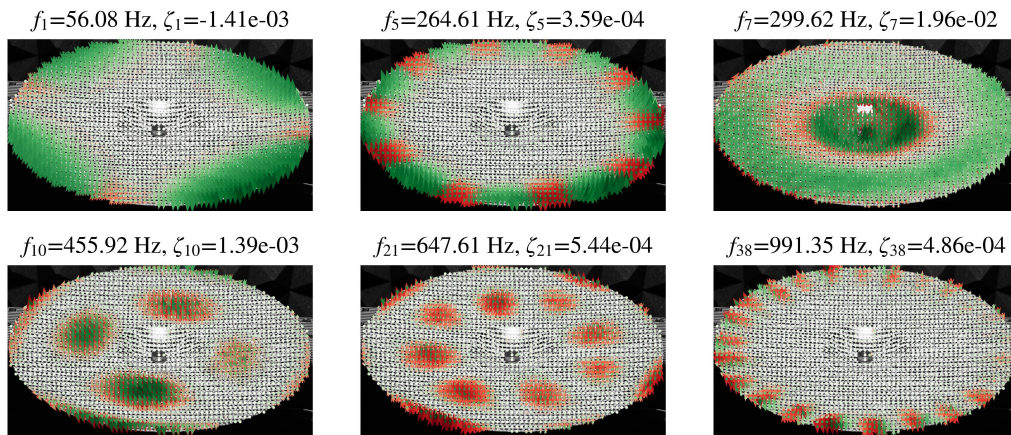


Figure 6: Set of dense identified mode shapes (1739 points) using the DSLR camera and SOFI.

The 39 identified modes for the point coincident to the position of the

accelerometer (see the red square in Figure 3) were then used to reconstruct the frequency-response function and compare it with the one measured by the accelerometer. The reconstructed response and the measured response are compared in Figure 7. Generally, the agreement between the responses is good. The accelerometer measurement and the SOFI measurement were performed as separate measurements for different excitation regimes and it is believed that the SOFI measurement was considerably influenced by the effect of non-linearities, due to an increased amplitude of the excitation that was used to make the displacements more evident to the camera, causing deviations from the accelerometer-only measurement. It should be noted that the maximum response amplitudes ranged from approximately four pixels in the case of the first two modes down to only 0.01 pixel in the case of higher-end frequencies. Some of these small amplitudes appear to be very close to the noise floor. Also, some of the points with the higher-amplitude displacements of the first two modes might have violated the small-motion assumption.

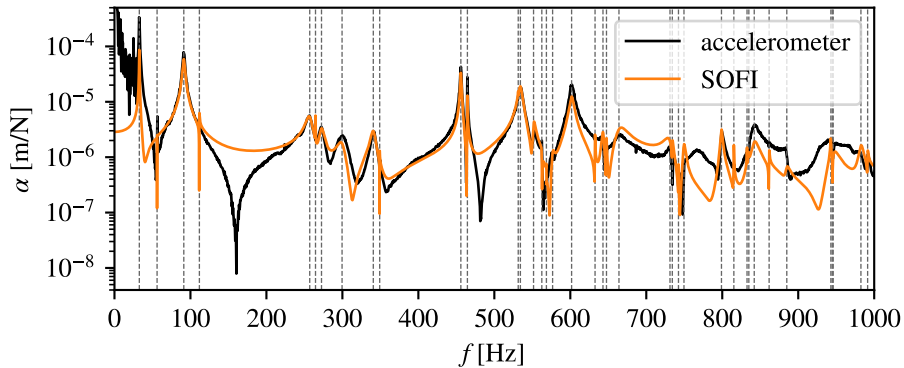


Figure 7: Comparison of the frequency response measured by the accelerometer and the response identified using SOFI in the hybrid modal-parameter identification. The vertical dotted lines indicate the identified resonant frequencies.

## 6. Conclusion

Still-frame cameras produce higher-resolution images at a lower cost. By using spectral optical flow imaging (SOFI), displacements caused by high

frequency oscillations can be measured far above the camera's frame rate. Using aliasing approaches demonstrated in works [9–11] at frequencies so far above the Nyquist frequency, would produce a very cluttered spectrum and probably an increase in uncertainty. In SOFI a harmonically time-varying illumination modulates the displacements and the camera integrates them over time, thereby producing the displacement spectral components over the entire image. In this paper the SOFI full-field displacement fields were used along with an accelerometer/laser-vibrometer measurement to identify the full-field mode shapes with a hybrid modal-parameter identification. The proposed approach was successful in identifying the modal parameters from which the response functions for the full-field can be produced and are in agreement with the accelerometer measurement. To produce satisfactory results, appropriate conditions have to be met: the illumination has to vary harmonically, the displacement should be small and no camera motion should be present. The camera motion proved to be the greatest problem, because it seems that the camera's shutter operation produces shifts in the lens optics between frames. So, instead of capturing still-frames a continuous video was filmed and decomposed into separate SOFI images.

## 7. Acknowledgement

The authors acknowledge the partial financial support from the Slovenian Research Agency (research core funding No. P2-0263 and J2-6763).

- [1] J. Javh, J. Slavič, M. Boltežar, The subpixel resolution of optical-flow-based modal analysis, *Mechanical Systems and Signal Processing* 88 (2017) 89–99.
- [2] B. Lucas, T. Kanade, An iterative image registration technique with an application to stereo vision, *International Joint Conference on Artificial Intelligence* (1981) 674–679.
- [3] T. J. Bebernis, D. A. Ehrhardt, High-speed 3D digital image correlation vibration measurement: Recent advancements and noted limitations, *Mechanical Systems and Signal Processing* 86 (2017) 35–48.

- [4] D. A. Ehrhardt, M. S. Allen, S. Yang, T. J. Beberniss, Full-field linear and nonlinear measurements using continuous-scan laser doppler vibrometry and high speed three-dimensional digital image correlation, *Mechanical Systems and Signal Processing* 86 (2017) 82–97.
- [5] J. Baqersad, P. Poozesh, C. Niezrecki, P. Avitabile, A noncontacting approach for full-field strain monitoring of rotating structures, *Journal of Vibration and Acoustics* 138 (3) (2016) 031008.
- [6] P. Poozesh, J. Baqersad, C. Niezrecki, P. Avitabile, E. Harvey, R. Yarala, Large-area photogrammetry based testing of wind turbine blades, *Mechanical Systems and Signal Processing* 86 (2017) 98–115.
- [7] D. Feng, M. Q. Feng, Experimental validation of cost-effective vision-based structural health monitoring, *Mechanical Systems and Signal Processing* 88 (2017) 199–211.
- [8] X. Zhao, K. Ri, N. Wang, Experimental verification for cable force estimation using handheld shooting of smartphones, *Journal of Sensors* 2017 (5625396).
- [9] Y. Liu, H. Gao, J. Zhuge, J. Zhao, Research of under-sampling technique for digital image correlation in vibration measurement, *Shock & Vibration, Aircraft/Aerospace, Energy Harvesting, Acoustics & Optics* 9 (2017) 49–58.
- [10] J. Javh, M. Brumat, J. Slavič, M. Boltežar, A high-speed camera measurement set-up for deflection shape analysis, *Proceeding of ISMA2016-USD2016* (2016) 1043–1050.
- [11] Y. Yang, C. Dorn, T. Mancini, Z. Talken, S. Nagarajaiah, G. Kenyon, C. Farrar, D. Mascarenas, Blind identification of full-field vibration modes of output-only structures from uniformly-sampled, possibly temporally-aliased (sub-Nyquist), video measurements, *Journal of Sound and Vibration* 390 (2017) 232–256.
- [12] A. Davis, M. Rubinstein, N. Wadhwa, G. Mysore, F. Durand, W. T. Freeman, The visual microphone: Passive recovery of sound from video, *ACM Transactions on Graphics (Proc. SIGGRAPH)* 33 (4) (2014) 1–10.

- [13] S. Stampfer, *Die stroboscopischen Scheiben; oder, Optischen Zauberscheiben: Deren Theorie und wissenschaftliche Anwendung*, Trentsensky & Vieweg, 1833.
- [14] T. G. Ryall, C. S. Fraser, Determination of structural modes of vibration using digital photogrammetry, *Journal of aircraft* 39 (1) (2002) 114–119.
- [15] A. Molina-Viedma, L. Felipe-Sesé, E. López-Alba, F. Díaz, High frequency mode shapes characterisation using digital image correlation and phase-based motion magnification, *Mechanical Systems and Signal Processing* 102 (2018) 245–261.
- [16] L. Yu, B. Pan, Single-camera high-speed stereo-digital image correlation for full-field vibration measurement, *Mechanical Systems and Signal Processing* 94 (2017) 374–383.
- [17] Y. Chi, L. Yu, B. Pan, Low-cost, portable, robust and high-resolution single-camera stereo-dic system and its application in high-temperature deformation measurements, *Optics and Lasers in Engineering* 104 (2017) 141–148.
- [18] M. Pankow, B. Justusson, A. M. Waas, Three-dimensional digital image correlation technique using single high-speed camera for measuring large out-of-plane displacements at high framing rates, *Applied Optics* 49 (17) (2010) 3418–3427.
- [19] J. Javh, J. Slavič, M. Boltežar, Measuring full-field displacement spectral components using photographs taken with a dslr camera via an analogue fourier integral, *Mechanical Systems and Signal Processing* 100 (2018) 17–27.
- [20] J. Javh, J. Slavič, M. Boltežar, High frequency modal identification on noisy high-speed camera data, *Mechanical Systems and Signal Processing* 98 (2018) 344–351.
- [21] P. Guillaume, P. Verboven, S. Vanlanduit, Frequency-domain maximum likelihood identification of modal parameters with confidence intervals, *Proceedings of ISMA* 23 (1998) 16–18.

- [22] H. V. Auweraer, W. Leurs, P. Mas, L. Hermans, Modal parameter estimation from inconsistent data sets, *Proceeding of IMAC XVIII (2000)* 763–771.
- [23] K. Shin, J. Hammond, *Fundamentals of signal processing for sound and vibration engineers*, John Wiley & Sons, 2008.
- [24] D. J. Ewins, *Modal Testing: Theory and Practice*, John Wiley & Sons, Ontario, Canada, 1984.
- [25] B. Cauberghe, *Applied frequency-domain system identification in the field of experimental and operational modal analysis*, Ph.D. thesis, Vrije Universiteit Brussel (2004).